International Journal of Mining Science and Technology 31 (2021) 421–428

Contents lists available at ScienceDirect

International Journal of Mining Science and Technology

journal homepage: www.elsevier.com/locate/ijmst

An improved form of smoothed particle hydrodynamics method for crack propagation simulation applied in rock mechanics

Shuyang Yu [a], Xuhua Ren [a,*], Jixun Zhang [a], Haijun Wang [b], Zhaohua Sun [c]

[a] College of Water Conservancy and Hydropower Engineering, Hohai University, Nanjing 210098, China
[b] State Key Laboratory of Hydrology-Water Resource and Hydraulic Engineering, Nanjing Hydraulic Research Institute, Nanjing 210029, China
[c] School of Transportation and Civil Engineering, Nantong University, Nantong 226019, China

ARTICLE INFO

Article history:
Received 20 August 2020
Received in revised form 9 December 2020
Accepted 26 January 2021
Available online 12 February 2021

Keywords:
IKSPH
Kernel function
Crack propagation
Fracture mechanics
Numerical simulation

ABSTRACT

The simulation of crack propagation processes in rock engineering has been not only a research hot spot among scholars but also a challenge. Based on this background, a new numerical method named improved kernel of smoothed particle hydrodynamics (IKSPH) has been put forward. By improving the kernel function in the traditional smoothed particle hydrodynamics (SPH) method, the brittle fracture characteristics of the base particles are realized. The particle domain searching method (PDSM) has also been put forward to generate the arbitrary complex fissure networks. Three numerical examples are analyzed to validate the efficiency of IKSPH and PDSM, which can correctly reveal the morphology of wing crack and the laws of crack coalescence compared with previous experimental and numerical studies. Finally, a rock slope model with complex joints is numerically simulated and the progressive failure processes are exhibited, which indicates that the IKSPH method can be well applied to rock mechanics engineering. The research results showed that IKSPH method reduces the programming difficulties and avoids the traditional grid distortion, which can provide some references for the application of IKSPH to rock mechanics engineering and the understanding of rock fracture mechanisms.

1. Introduction

Rock is a typical anisotropic material, which contains large amounts of inherent defects with relatively lower strength. These defects include faults, fissures, joints, holes, interlayers and so on, which makes rock exhibit the characteristics of heterogeneity, non-linearity, and strong discontinuity [1]. Furthermore, under complex multi-field coupling conditions [2], the rock structures may fail due to these defects. Therefore, how to correctly describe the discontinuous characteristics of rock masses has been a hot but difficult problem in recent years.

As an important supplement and extension of experimental research and theoretical model, numerical simulation has developed into the third method of scientific research [3,4]. Compared with the complexities of experimental research and the limitations of theoretical research [5], numerical simulation can give accurate solutions and predictions as long as reasonable constitutive relations and calculation parameters are given. Hence, the simulation of the heterogeneity and discontinuity of rock structures has been more and more popular among scholars all over the world.

The finite element method (FEM) is one of the earliest numerical methods to study the rock fracture mechanics. However, uncertainties exist in the crack propagation directions [6], in other words, the crack propagation direction is not previously known. As a consequence, FEM needs to change the grid division of crack tips at every time step. Early researches on crack propagation of rock materials mainly included two types, namely mesh re-division method [7,8] and the joint interface element method [9]. The mesh re-division method has a high demand for the quality of the mesh division, so the complex crack mesh will be extremely distorted, leading to the inaccuracy of the calculation results or even the calculation failure. The interface element method is sensitive to the shape and size of the mesh. Meanwhile, this method costs huge amounts of calculation time. In order to solve these problems, the cohesive element method has been put forward to model the rock failure processes [10,11]. However, there exists some disadvantages such as difficulties in convergence and poor adaptability of mesh. The extended finite element method (XFEM), which is regarded as an improved FEM, has been widely used since it was proposed in the 1990 s [12,13]. This method uses enrichment functions to describe the geometry of cracks. Nonetheless, for complex crack geometries such as 3D internal cracks or multiple intersecting cracks, the applications of XFEM are still limited [14].

* Corresponding author.
E-mail address: renxh@hhu.edu.cn (X. Ren).

https://doi.org/10.1016/j.ijmst.2021.01.009
2095-2686/

The discrete element method (DEM) is another effective numerical simulation method developed after FEM [15,16], which utilizes various contact models between particles to model the whole crack initiation and propagation process. The most representative commercial softwares such as PFC2D and PFC3D developed by Itasca have been widely used in the simulations of experimental samples or even the rock mechanics engineering [17–21]. However, the DEM method needs to establish the relationship between the macro and micro parameters through parameter calibration, where large amounts of micro parameters are requested [22]. Meanwhile, the DEM method still has some problems in solving continuous problems [23].

Recent numerical methods such as numerical manifold method (NMM) [24–26], peridynamics (PD) [27–29], material point method (MPM) [30,31], isogeometric-meshfree coupling approach [32–35], and phase-field modeling [36,37], all have their unique advantages in solving rock fracture mechanics with large deformation and high non-linearity, but still have some limitations. For example, the crack tips can not be inside the element in the NMM method [38]; the bond-based PD method has some theoretical defects, which leads to the Poisson's ratio being constant [39]; the MPM method needs to match the material points through background grids [40].

The smoothed particle hydrodynamics (SPH) is a pure Lagrange mesh-less numerical method, which was originally used in astrophysical problems [41,42]. Subsequently, it has been widely applied in solving complex fluid dynamics problems [43,44]. Due to its Lagrangian properties, it has a unique advantage in dealing with problems of large deformations and discontinuities. Hence, in recent years, it has been utilized in the rock fracture mechanics. One of the most representative works is the general particle dynamics (GPD) method developed by Zhou and his co-workers [5,45,46]. In their work, the 2D and 3D rock fracture programs based on SPH method were developed, of which the core was based on the principle of stiffness reduction; the improved GPD method was used in solving the water-stress coupling problems, which is based on the fracture of the stress bond [47–49].

The aim of this paper is to put forward a more simplified but effective numerical method called improved kernel of smoothed particle hydrodynamics (IKSPH) to model the fracture process in rock mechanics. Numerical models consist of base particles rather than meshes so it can avoid the mesh distortion. The key of the proposed method is improving the derivative of the kernel function in the traditional SPH method. By adding a fracture mark variable ξ, the base particles satisfying the fracture criterion no longer transmit the parameter information to the surrounding base particles, thus realizing the brittle fracture characteristics of the rock material. Meanwhile, the particle domain searching method (PDSM) has also been proposed to realize the formation of complex fissure networks, which is easy and effective to operate. Compared with previous SPH methods [47–49], the stress components of the base particles do not need to be mapped to the stress bond, which reduces the programming amount. Meanwhile, the arbitrary crack shapes can be easily generated. Four numerical examples are carried out to validate the proposed methods. The research results can provide some references for the applications of SPH method to rock fracture mechanics and the understanding of the mechanisms of crack propagation as well as the crack interaction.

2. Basic IKSPH

2.1. Governing equations

Each unit point in IKSPH is called base particle, which records all the calculation parameters and result information at every time step. For each base particle, the governing equations include four parts, namely (1) continuity equation, (2) momentum equation, (3) energy equation, and (4) motion equation, which can be expressed as [50,51]

$$\begin{cases} \mathrm{d}\rho_i/\mathrm{d}t = \sum_{j=1}^{N} m_j \boldsymbol{v}_{ij}\left(\partial \boldsymbol{W}_{ij}/\partial \boldsymbol{x}_i\right) \\ \mathrm{d}\boldsymbol{v}_i/\mathrm{d}t = \sum_{j=1}^{N} m_j(\boldsymbol{\sigma}_i/\rho_i^2 + \boldsymbol{\sigma}_j/\rho_j^2 + T_{ij})\left(\partial \boldsymbol{W}_{ij}/\partial \boldsymbol{x}_i\right) \\ \mathrm{d}e_i/\mathrm{d}t = \frac{1}{2}\sum_{j=1}^{N} m_j(\boldsymbol{\sigma}_i/\rho_i^2 + \boldsymbol{\sigma}_j/\rho_j^2 + T_{ij})\boldsymbol{v}_{ij}\left(\partial \boldsymbol{W}_{ij}/\partial \boldsymbol{x}_i\right) \\ \mathrm{d}\boldsymbol{x}_i/\mathrm{d}t = \boldsymbol{v}_i \end{cases} \tag{1}$$

where i is the base particle number; j the base particles which are within the influencing range of base particle i; N the counts of base particle j; ρ_i and ρ_j the i-th and j-th base particle, respectively; t the calculation time; m_i and m_j the mass of the i-th and j-th base particle, respectively; $\boldsymbol{v}_i$ and $\boldsymbol{v}_j$ the velocity of the i-th and j-th base particle, respectively, $\boldsymbol{v}_{ij} = \boldsymbol{v}_j - \boldsymbol{v}_i$; $\boldsymbol{x}_i$ the position of the i-th base particle; $\boldsymbol{\sigma}_i$ and $\boldsymbol{\sigma}_j$ the total stress tensor of the i-th and j-th base particle; e_i the energy of the i-th base particle; T_i and T_j the artificial viscous part of i-th and j-th base particle, $T_{ij} = T_j - T_i$, which can reduce nonphysical oscillations during calculation [52]; and $\boldsymbol{W}_i$ and $\boldsymbol{W}_j$ the kernel function of the i-th and j-th base particle, $\boldsymbol{W}_{ij} = \boldsymbol{W}_j - \boldsymbol{W}_i$, which can be expressed as [53]

$$\boldsymbol{W}(s,h) = \begin{cases} 2/3 - s^2 + 1/(2s^3), & 0 \leqslant s < 1 \\ 1/\left(6(2-s)^3\right), & 1 \leqslant s < 2 \\ 0, & 2 \leqslant s \end{cases} \tag{2}$$

where h is the smoothing length; and s the ratio of the base particle distance and the smoothing length.

2.2. Constitutive equation

The total stress tensor $\boldsymbol{\sigma}$ consists of two parts: (1) the hydrostatic pressure p and (2) the shear stress $\boldsymbol{\tau}$. Therefore, $\boldsymbol{\sigma}$ can be expressed as

$$\boldsymbol{\sigma} = -p\boldsymbol{\delta} + \boldsymbol{\tau} \tag{3}$$

where $\boldsymbol{\delta}$ is the kronecker symbol; and p the hydrostatic pressure which can be estimated by the solid state equation of Mie-Grüneisen [51].

$$p = (1 - \Gamma\eta/2)p_{\mathrm{H}} + \Gamma\rho e \tag{4}$$

where p_{H} is the Hugoniot curve function; Γ the Grüneisen parameter; and $\eta = \rho/\rho_0 - 1$, where ρ_0 is the original value of base particle density.

For solid constitutive equation, stress is a function of strain and strain rate. By introducing Jaumann ratio, the stress rate can be expressed as follows.

$$\overset{\circ}{\boldsymbol{\tau}} = B(\boldsymbol{\varepsilon} - \boldsymbol{\delta\varepsilon}/3) + \boldsymbol{\tau R} \tag{5}$$

where $\overset{\circ}{\boldsymbol{\tau}}$ is the stress rate tensor; B the shear modulus; $\boldsymbol{\varepsilon}$ the strain tensor of the base particle; and $\boldsymbol{R}$ the torsion tensor.

2.3. Time integration

IKSPH method uses the leapfrog (LF) algorithm to integrate the discretized equation. The advantage is that the storage required in the calculation is lower, and only one optimization valuation is needed in every calculation step. For each base particle, its position, velocity, density, and energy are recursively obtained by Eq. (6).

$$\begin{cases} t = t_0 + \Delta t \\ \rho_i(t_0 + \Delta t/2) = \rho_i(t_0) + (\Delta t/2)\Delta\rho_i(t_0) \\ e_i(t_0 + \Delta t/2) = e_i(t_0) + (\Delta t/2)\Delta e_i(t_0) \\ \boldsymbol{v}_i(t_0 + \Delta t/2) = \boldsymbol{v}_i(t_0) + (\Delta t/2)\Delta \boldsymbol{v}_i(t_0) \\ \boldsymbol{x}_i(t_0 + \Delta t) = \boldsymbol{x}_i(t_0) + \Delta t \boldsymbol{v}_i(\Delta t/2) \end{cases} \tag{6}$$

where t_0 is the original time; and Δt the time step.

2.4. Quadrature rules

One key difference between the FEM and IKSPH method is that IKSPH discretizes the solution space of the problem domain into a region consisting of a number of base particles. Each base particle has an influencing domain, and then the properties of each base particle are calculated according to the approximation method expressed as follows.

$$f(\boldsymbol{x}_i) = \sum_{j=1}^{N} \left(m_j/\rho_j\right) f(\boldsymbol{x}_j) \boldsymbol{W}(\boldsymbol{x}_i - \boldsymbol{x}_j, h) \tag{7}$$

where f is the property function of base particles.

3. Fracture treatments in IKSPH

3.1. Fracture criteria

For all the base particles, they exchange parameter information through the derivatives of the smoothing kernel functions in their support domains, in other words, the kernel functions of each base particle and their derivatives are the "communication bridges" among all the base particles. Therefore, for each base particle, it is only necessary to improve the smoothing kernel function and its derivative so that it can "cut off" the bridge in the supporting domain in time when the base particle is damaged, which can correctly reflect the brittle fracture characteristics of rock materials, as shown in Fig. 1.

The failure of the base particle follows the Mohr-Coulomb criterion with a tension cut off [54], which has been widely used in the previous numerical simulations of fracture mechanics and has achieved good results. It can be expressed as

$$\sigma_f = \sigma_t \tag{8}$$

$$\tau_f = c + \sigma_f \tan\varphi \tag{9}$$

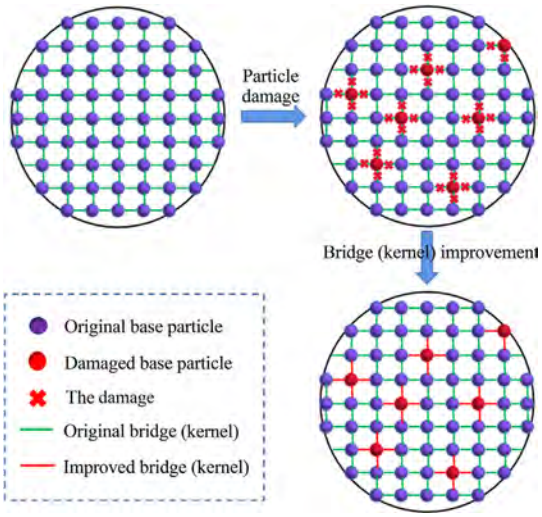

Fig. 1. Fracture of the base particle.

where σ_f and τ_f are the maximum tensile stress and shear stress of the failure surface, respectively; σ_t the tensile strength of the base particle; c the cohesion of the base particle; and φ the internal friction angle of the base particle. What should be noticed is that when the base particle satisfies the tensile failure criteria (Eq. (8)), the tensile failure first happens. If Eq. (8) is not satisfied, then IKSPH judges whether Eq. (9) is satisfied, which means the shear failure.

For each base particle, when Eq. (8) or Eq. (9) is satisfied, the base particle is damaged, and no longer transmits the parameter information with other base particles. According to the IKSPH governing equation (Eq. (1)), the derivative of smoothing kernel function plays an important role in linking different base particles. So it is necessary to improve the kernel function. Here a fracture mark variable ξ is introduced in the IKSPH programme. During each cycle, the fracture state of each base particle is judged, if Eqs. (8) and (9) are not satisfied, then ξ = 1, and when Eq. (8) or Eq. (9) is satisfied, then ξ = 0.

Therefore, as for the derivative of kernel function in Eq. (1), considering the brittle fracture characteristics of the base point, its improved form can be expressed as

$$\partial \boldsymbol{D}_{ij}/\partial \boldsymbol{x}_i = \xi_i \cdot \left(\partial \boldsymbol{W}_{ij}/\partial \boldsymbol{x}_i\right) \tag{10}$$

where $\boldsymbol{D}$ is the improved form of kernel function considering the brittle fracture characteristics of the base particle, $\boldsymbol{D}_{ij} = \boldsymbol{D}_j - \boldsymbol{D}_i$. Hence the modified IKSPH governing equations can be re-written as

$$\begin{cases} \mathrm{d}\rho_i/\mathrm{d}t = \sum_{j=1}^{N} m_j \boldsymbol{v}_{ij} \left(\partial \boldsymbol{D}_{ij}/\partial \boldsymbol{x}_i\right) \\ \mathrm{d}\boldsymbol{v}_i/\mathrm{d}t = \sum_{j=1}^{N} m_j (\boldsymbol{\sigma}_i/\rho_i^2 + \boldsymbol{\sigma}_j/\rho_j^2 + T_{ij}) \left(\partial \boldsymbol{D}_{ij}/\partial \boldsymbol{x}_i\right) \\ \mathrm{d}e_i/\mathrm{d}t = \frac{1}{2} \sum_{j=1}^{N} m_j (\boldsymbol{\sigma}_i/\rho_i^2 + \boldsymbol{\sigma}_j/\rho_j^2 + T_{ij}) \boldsymbol{v}_{ij} \left(\partial \boldsymbol{D}_{ij}/\partial \boldsymbol{x}_i\right) \\ \mathrm{d}\boldsymbol{x}_i/\mathrm{d}t = \boldsymbol{v}_i \end{cases} \tag{11}$$

3.2. Particle domain searching method (PDSM)

For traditional FEM, the generation of complex fissure networks are accompanied by complex mesh divisions, or the complex expressions of the crack surface. For staggered multi-fissure systems, it usually takes a lot of time to apply finite element mesh pre-treatments, or even can not be subdivided. Even if the subdivision is successful, it may be impossible to calculate due to the extreme distortion of the grids. As for IKSPH, due to its excellent Lagrangian characteristics, the previous works requiring special treatments of the cracks no longer exist in this new numerical method.

For multi fissures and complex fracture morphology, the particle domain searching method (PDSM) is introduced here to generate fissure networks, as shown in Fig. 2. Firstly, the arbitrary fissure lines l_i (i = 1, 2, …, n) are generated within the domain Ω of the base particles (one typical example is the three cyan lines in Fig. 2). Secondly, we generate m_i searching particles (the yellow points in Fig. 2) uniformly on each fissure line l_i. Thirdly, for each searching particle $m_i \in l_i$, the searching radius r_d is set, which is generally taken as the value of smoothing length h. If the base particle is covered by the searching domain Ω_i formed by the searching radius r_d, the base particle is then marked as the fissure base particle. Finally, the fissure base particles can be directly deleted or processed according to the method in Section 3.1. Therefore, the arbitrary fissure networks can be generated by doing the loops for each searching particle.

To summarize, the calculation process can be expressed as follows.

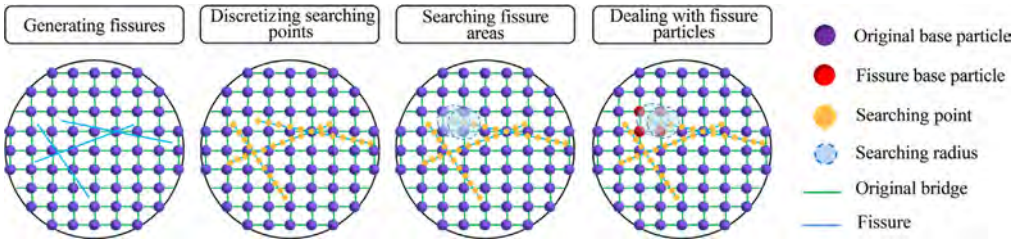

Fig. 2. Particle domain searching method (PDSM).

(1) Input initialization information of base particles, including the coordinates, initial velocities, initial stress, boundary conditions, etc.
(2) Define the basic information of the fracture networks, including the two endpoints of each crack and the searching particle dispersion of each crack line.
(3) For each discrete searching particle, the searching loops are carried out with a smoothing length h as the radius. If the base particle is covered by the searching domain formed by the searching radius, the base particle is then marked as the fissure base particle, and the fissure base particles can be directly deleted or processed according to the method in Section 3.1.
(4) The particle searching is performed at each time step (the link-list searching algorithm [55] is applied here in this paper), and the smoothing kernel function of each base particle pair is then updated.
(5) The density, stress, and energy are updated according to Eqs. (3) and (11).
(6) The fracture state of each base particle is judged according to Eqs. (8) and (9).
(7) The velocity and position of each base particle are updated, and if the programme is not finished, return to step (3).

4. Boundary treatment

Due to the inherent defects of the base particles on or near the boundary (whose influencing domains are truncated when integrating, as shown in Fig. 3), it is necessary to treat the boundary part to improve the computational accuracy. The virtual particles are then introduced here to realize a better physical meaning of the boundary. As suggested by [56], there are two types of virtual particles, one type is type I virtual particle, which is set on the fixed boundary, as shown in Fig. 3, and the other type is type II virtual particle, which is set outside the boundary and symmetrically distributed with respect to the real base particle. The repulsive force P_r exerted by the type I virtual particle on the real base particle can be expressed as follows.

$$P_r = \begin{cases} \chi\left[(r_0/r_{ij})^{q_1} - (r_0/r_{ij})^{q_2}\right]\left(x_{ij}/r_{ij}^2\right), & r_0/r_{ij} < 1 \\ 0, & r_0/r_{ij} \geqslant 1 \end{cases} \tag{12}$$

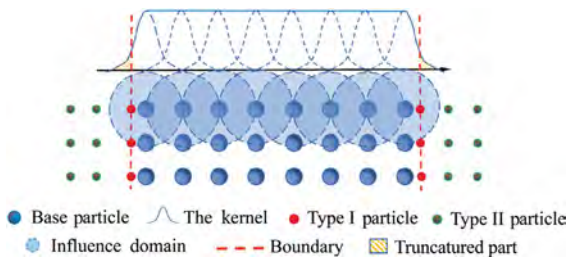

Fig. 3. Boundary virtual particles.

where χ is the repulsive force factor, which is generally taken to be the square of the maximum velocity; r_0 the average distance between the base particles; r_{ij} the distance between the real base particle and the type I virtual particle, $r_{ij} = r_j - r_i$; and q_1 and q_2 are set to 12 and 4, respectively.

5. Examples and discussions

In order to verify the IKSPH numerical method proposed in this paper, four numerical examples are simulated, and the results are compared with the existing experimental results or numerical simulation results. The example 1 is the numerical simulation of the crack growth process under uniaxial compression of a standard cube sample with one single inclined fissure. The example 2 is the numerical simulation of the crack growth process under uniaxial compression of a standard cube sample with two inclined fissures. The example 3 is the numerical simulation of the uniaxial compression of specimens containing two pre-existing fissures. The example 4 is an engineering simulation: the progressive failure process of a jointed rock slope under the load of self-weight, so as to show that IKSPH can be applied to the rock mechanics engineering. The main purpose of these numerical examples is to show the progressive failure process, crack morphology, and crack interaction law, so the numerical parameters are not strictly calibrated, and the elastic parameters of the model are set to be consistent. The density ρ = 2600 kg/m^3, elastic modulus E = 17 GPa, and Poisson's ratio μ = 0.14.

5.1. Numerical simulation of compression and shear failure with one single crack

The numerical example 1 comes from [57], which is shown in Fig. 4. The sample is a standard cube specimen with a length of 50 mm and a height of 100 mm. A 15 mm long fissure is prefabricated at the center of the specimen, and the angle between the fissure and the horizontal direction is 45°. The whole sample is discretized into 12675 base particles. The model adopts displacement loading mode, the loading rate is 5×10^{-3} m/s, and the calculation time step is 1×10^{-8} s. The cohesion c is set to 5.95 MPa, the internal friction angle φ is set to 40°, and the tensile strength σ_t is set to 2 MPa.

The progressive failure process of the sample is shown in Fig. 5a. As can be seen, wing crack originates from the crack tips and then propagates along the loading direction, and the stress concentrates on the crack tips. The crack morphology is consistent with the experimental results (DIC) [57], which verifies the accuracy of the proposed IKSPH method. The theoretical model in Fig. 5b shows that the formation of wing crack is due to the slip and dislocation of the upper and lower crack surfaces, and the wing crack widens during its propagation, which indicates that the compress and shear action of prefabricated cracks will make the wing crack surface open, and the numerical results can reveal this phenomenon.

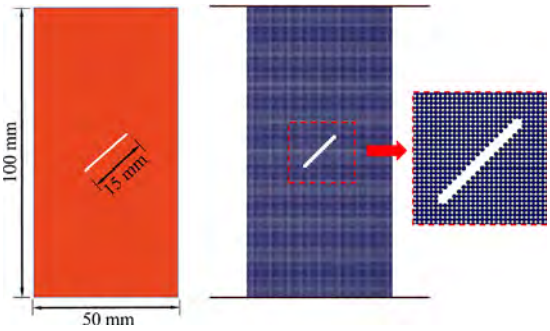

Fig. 4. Model size and base particle distribution of example 1.

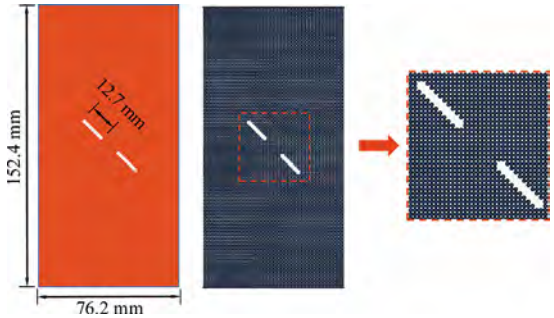

Fig. 6. Model size and base particle distribution of example 2.

5.2. Numerical simulation of compression and shear failure with two cracks

The numerical example 2 comes from [58], which is shown in Fig. 6. The sample is a standard cube specimen with a length of 76.2 mm and a height of 152.4 mm. Two 12.7 mm long fissures are prefabricated at the center of the specimen, and the angle between the fissure and the horizontal direction is 45°. The whole sample is discretized into 12738 base particles. The model adopts displacement loading mode, the loading rate is 5×10^{-3} m/s, and the calculation time step is 1×10^{-8} s. The cohesion c is set to 5.95 MPa, the internal friction angle φ is set to 40°, and the tensile strength σ_t is set to 2 MPa.

The progressive failure process of the sample is shown in Fig. 7a. As can be seen, the typical wing crack originates from the crack tips just similar to example 1. However, the crack propagation of inner side is less than that of the outer side. The shear crack occurs in the inner tips of two fissures, which is consistent with the experimental results in [58].

5.3. Numerical simulation of compression and shear failure with multiple cracks

The numerical example 3 comes from [59], which is shown in Fig. 8. The sample is a standard cube specimen with a length of 150 mm and a height of 300 mm. A total number of 15 inclined cracks are prefabricated at equal intervals. The length of the prefabricated crack is L = 40 mm, the transverse spacing is C = 45 mm, the longitudinal spacing is S = 40 mm, and the inclination angle is α = 45°. The whole sample is discretized into 11570 base particles. The model adopts displacement loading mode and the loading rate is 5×10^{-3} m/s, and the calculation time step is 5×10^{-8} s. The cohesion c is set to 5.95 MPa, the internal friction angle φ is set to 40°, and the tensile strength σ_t is set to 2 MPa.

The progressive failure process of the sample is shown in Fig. 9. As can be seen, the wing crack propagates the most in the middle of the sample, but the least on the left and right side. The propagation and overlap of wing crack result in the interlacing of the joints in the fractured rock masses, which is highly consistent with the

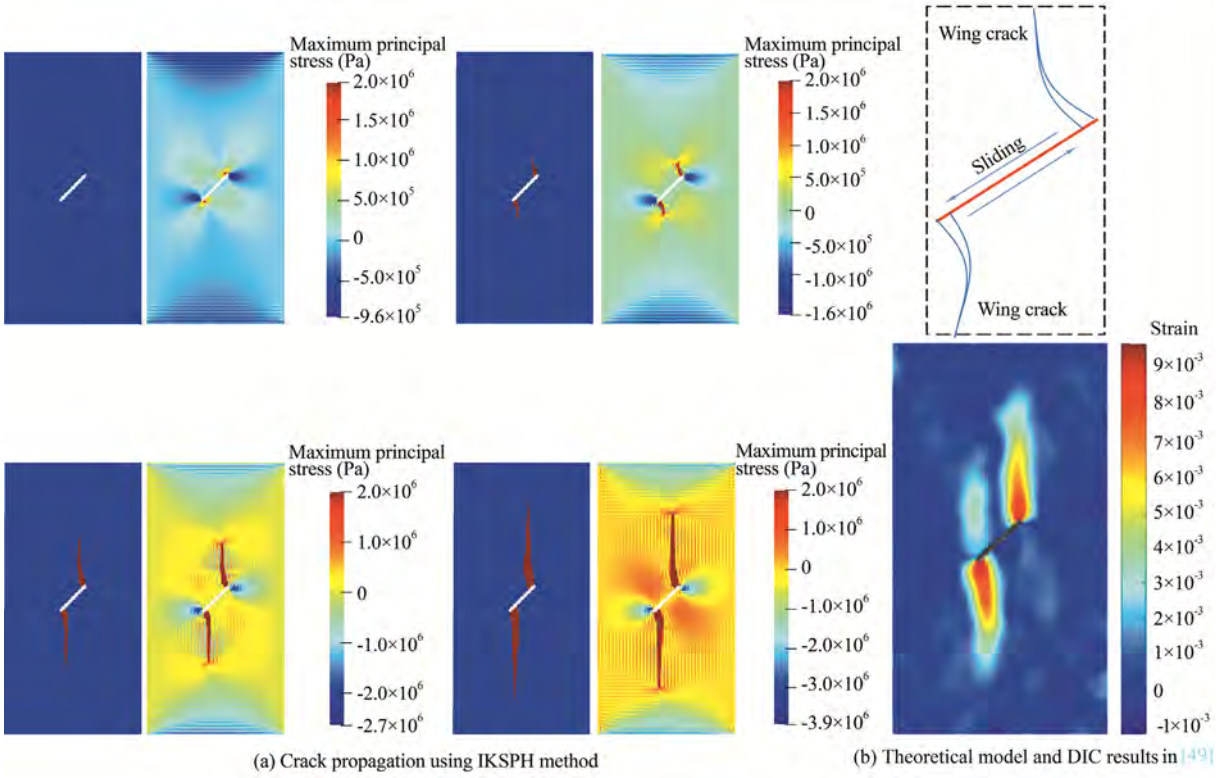

Fig. 5. Crack propagation process of example 1 and its comparison with previous studies.

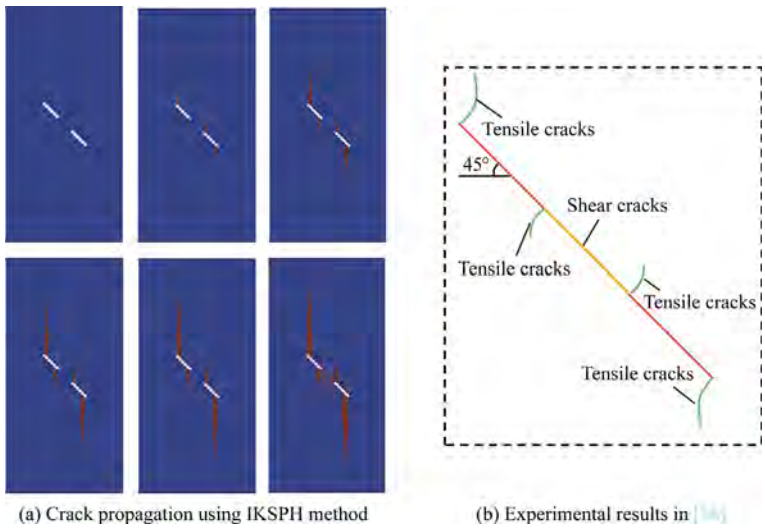

Fig. 7. Crack propagation process of example 2 and its comparison with previous studies.

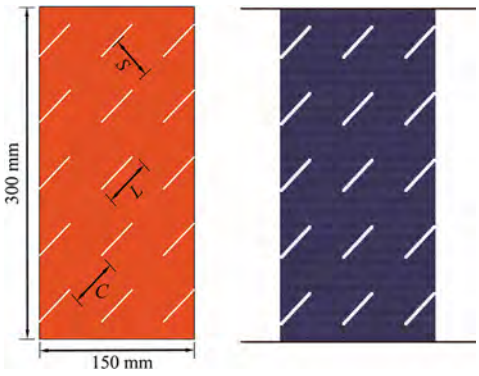

Fig. 8. Model size and base particle distribution of example 3.

experimental results in [59]. Thus, the accuracy and authenticity of IKSPH in the numerical simulation of crack propagation in rock masses are verified.

5.4. Numerical simulation of progressive failure of a typical jointed rock slope

The numerical example 4 comes from [14], which is a rock slope with non-persistent joints. The model size is shown in Fig. 10. The overloading method is used to apply the gravity load on the rock slope. The calculation time step is 1×10^{-8} s. The cohesion c is set to 6 MPa, the internal friction angle φ is set to 40°, the tensile strength σ_t is set to 0.3 MPa and the whole model is discretized into 11570 base particles.

The progressive failure process of the rock slope is shown in Fig. 11. Fig. 11a shows the failure process of the base particle, and Fig. 11b shows the distribution of maximum principal stress. The crack is first generated along the joint surface, and the slope toe is firstly destroyed. Finally it forms an obvious sliding surface. The joints divide the slope into several fragments, which is consistent with the numerical results in [14]. Therefore, the IKSPH method proposed in this paper can be well applied to rock mechanics engineering practice.

5.5. Computational cost analysis

The computational cost is one key index to characterize the computational efficiency of the proposed method. In order to investigate the computational cost of IKSPH, a typical cube specimen model with a length of 50 mm and a height of 100 mm is calculated. Different base particle numbers are set: (1) $50 \times 100 = 5000$ base particles, (2) $70 \times 140 = 9800$ base particles, (3) $100 \times 200 = 20000$ base particles, (4) $120 \times 240 = 28800$ base particles, and (5) $140 \times 280 = 39200$ base particles. 1000 calculation steps are adopted in each calculation condition. The hardware environment of the IKSPH program in this paper is DELL T5400, the CPU used is Intel(R) Core(TM) i5-6500 CPU @3.20 GHz 3.19 GHz, and the memory is 4.00 GB.

Fig. 12 shows the calculation cost under different particle numbers. The calculation time increases exponentially with the

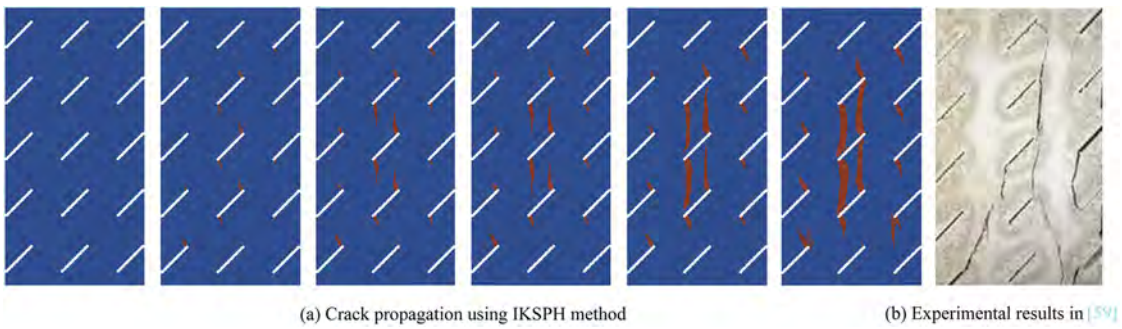

Fig. 9. Crack propagation process of example 3 and its comparison with previous studies.

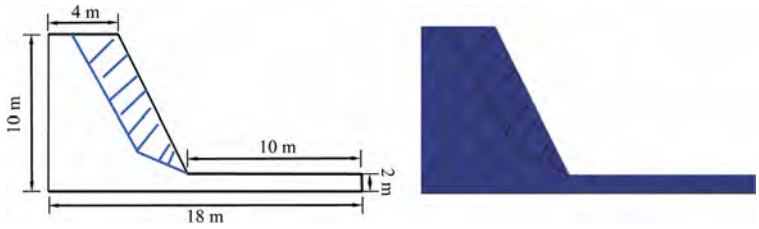

Fig. 10. Model size and base particle distribution of example 4.

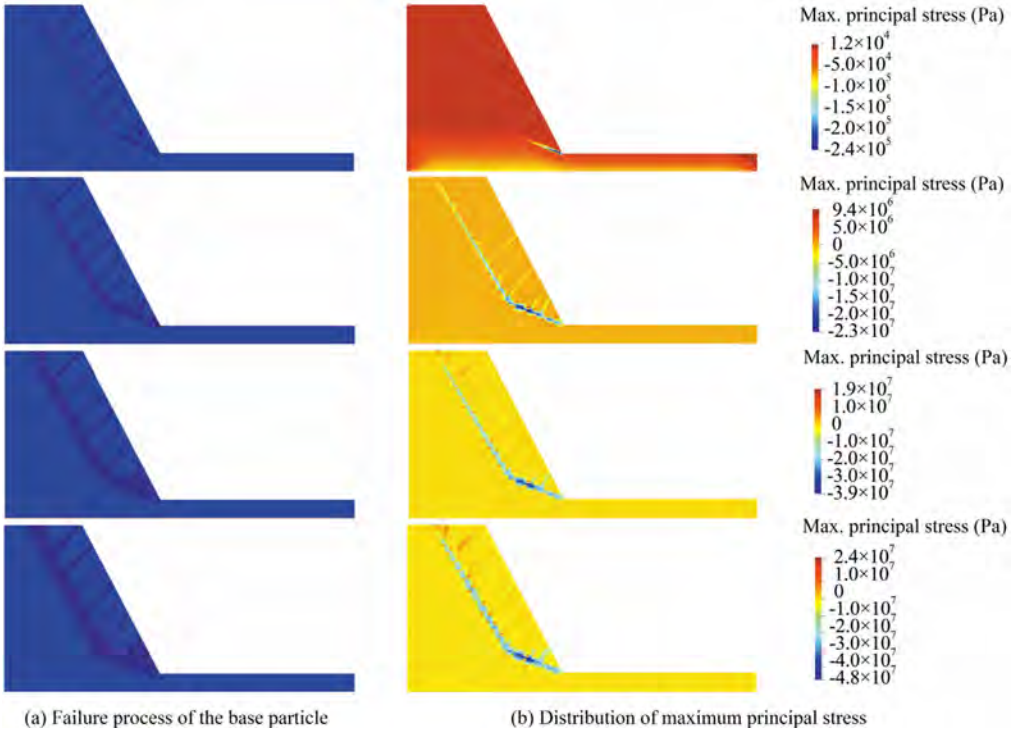

Fig. 11. Progressive failure process of example 4.

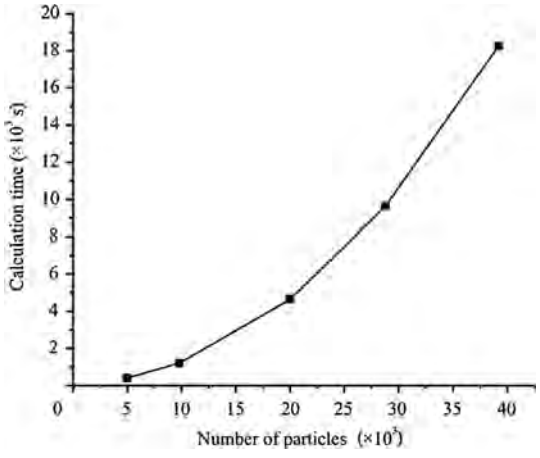

Fig. 12. Calculation cost under different particle numbers.

increase of particle number. We can see that when the particle number is approaching 40000, the calculation time is more than 5 h in 1000 steps, which is unacceptable. Therefore, more emphasis should be put on the parallel computing to improve the calculation efficiency.

6. Conclusions

(1) A new numerical method named improved kernel of smoothed particle hydrodynamics (IKSPH), which is aimed at modeling the brittle fracture of rock masses, has been proposed in this paper. Compared with previous studies, there is no need to reduce the stiffness of the base point or map the stress to the stress bond between different base particles, which has reduced programming difficulties. Meanwhile, the particle domain searching method (PDSM) has also been put forward to generate complex fissure networks.

(2) The accuracy of the IKSPH method proposed in this paper is verified by comparing the numerical results of samples containing single or multiple cracks with the experimental and numerical results in the previous studies. At the same time, IKSPH can accurately simulate the opening phenomenon of wing crack surface caused by the compress and shear action of prefabricated cracks.

(3) A typical rock slope with multiple joints is taken as an example for modeling. The simulation results are consistent with previous studies, which lays a foundation for the application of IKSPH method to rock mechanics engineering practice.

(4) The calculation efficiency under large amounts of particles is now unacceptable, so future works should put more emphasis on the parallel computing both on CPU and GPU.

Acknowledgements

The authors acknowledge the financial supports of the National Natural Science Fund (Nos. U1765204 and 51409170). Meanwhile, the authors greatly wish to express their thanks to Professor Bi Jing, Wuwen Yao, and Yongchuan Yu for their technical supports in the IKSPH programming.

References

[1] Tian J, Xu D, Liu T. An experimental investigation of the fracturing behaviour of rock-like materials containing two V-shaped parallelogram flaws. Int J Min Sci Technol 2020;30(6):777–83.
[2] Li P, Fan H, Wang M. A closed-form solution for the 3D steady-state thermoporoelastic field in an infinite transversely isotropic rock weakened by an elliptical crack. Int J Rock Mech Min Sci 2020;129:104292.
[3] Tang C, Li L, Li W, Ma T. RFPA strength reduction method for stability analysis of geotechnical engineering. Chinese J Rock Mech Eng 2006;15(8):1522–30.
[4] Liang Z. Three-Dimensional Failure Process Analysis of Rock and Associated Numerical Tests. Doctoral dissertation. Dalian: Northeast University; 2005.
[5] Zhou X, Zhao Y, Qian Q. A novel meshless numerical method for modeling progressive failure processes of slopes. Eng Geol 2015;192:139–53.
[6] Yang S, Cao M, Ren X. 3D crack propagation by the numerical manifold method. Comput Struct 2018;194(1):116–29.
[7] Song J, Chen F, Wang F. Study on the characteristics of the fracture process zone in concrete crack propagation based on FRANC3D. Int J Earth Sci Eng 2015;8(2):849–53.
[8] Branco R, Antunes F, Costa J. A review on 3D-FE adaptive remeshing techniques for crack growth modelling. Eng Fract Mech 2015;141:170–95.
[9] Xu X, Needleman A. Numerical simulations of fast crack growth in brittle solids. J Mech Phys Solids 1994;42(9):1397–434.
[10] Pandolfi A, Guduru P, Ortiz M. Three dimensional cohesive-element analysis and experiments of dynamic fracture in C300 steel. Int J Solids Struct 2000;37 (27):3733–60.
[11] Chen C, Linzell D. Modeling end notched flexure tests to establish cohesive element Mode II fracture parameters. Eng Fract Mech 2010;77(8):1338–47.
[12] Belytschko T, Black T. Elastic crack growth in finite elements with minimal remeshing. Int J Numer Meth Eng 2015;45(5):601–20.
[13] Moës Nicolas, Dolbow J, Belytschko T. A finite element method for crack growth without remeshing. Int J Numer Meth Eng 1999;46:131–50.
[14] Yang S, Ma G, Ren X. Cover refinement of numerical manifold method for crack propagation simulation. Eng Anal Boundary Elem 2014;43(1):37–49.
[15] Ajayi K, Shahbazi K, Tukkaraja P, Katzenstein K. Numerical investigation of the effectiveness of radon control measures in cave mines. Int J Min Sci Technol 2019;29(3):469–75.
[16] Hadjigeorgiou J, Esmaieli K, Grenon M. Stability analysis of vertical excavations in hard rock by integrating a fracture system into a PFC model. Tunn Undergr Space Technol 2009;24(3):296–308.
[17] Wang J, Wei W, Zhang J. Numerical investigation on the caving mechanism with different standard deviations of top coal block size in LTCC. Int J Min Sci Technol 2020;30(5):583–91.
[18] Zhang L. Systematic Investigation of the Planar Shape of Rock Fractures using PFC3D Numerical Experiments. Can J Cardiol 2012;28(6):750–7.
[19] Zhang B, He Q, Lin Z. Experimental study on the flow behaviour of water-sand mixtures in fractured rock specimens. International Journal of Mining Science and Technology 2021;31(3):377–385.
[20] Li H, Yang C, Ding X. Weibull linear parallel bond model (WLPBM) for simulating micro-mechanical characteristics of heterogeneous rocks. Eng Anal Boundary Elem 2019;11(108):82–94.
[21] Park J, Song J. Numerical Simulation Of Direct Shear Test On Rock Joint Using Pfc3D. Micro Injection Mold 2008;17(1):27–31.
[22] Zhou J, Lan H, Zhang L. Novel grain-based model for simulation of brittle failure of Alxa porphyritic granite. Eng Geol 2019;251:100–14.
[23] Li X, Wang S, Ge S. A Study on Drum Cutting Properties with Full-scale Experiments and Numerical Simulations. Measurement 2018;114:25–36.
[24] Li G, Wang K, Tang C, Qian X. An NMM-based fluid-solid coupling model for simulating rock hydraulic fracturing process. Eng Fract Mech 2020;235 (8):107–93.
[25] Ohnishi Y, Sasaki T, Koyama T. Recent insights into analytical precision and modelling of DDA and NMM for practical problems. Geomech Geoeng 2014;9 (2):97–112.
[26] Miki S, Sasaki T, Koyama T. Development of coupled discontinuous deformation analysis and numerical manifold method (NMM–DDA). Int J Comput Meth 2010;7(01):131–50.
[27] Shou Y, Zhou X, Qian Q. Dynamic Model of the Zonal Disintegration of Rock Surrounding a Deep Spherical Cavity. Int J Geomech 2016;17(6):04016127.
[28] Zhou X, Shou Y. Numerical Simulation of Failure of Rock-Like Material Subjected to Compressive Loads Using Improved Peridynamic Method. Int J Geomech 2016;22(3):04016086.
[29] Zhou X, Shou Y, Qian Q. Three-Dimensional Nonlinear Dynamic Strength Criterion for Rock. Int J Geomech 2016;16(2):04015041.
[30] Müller A, Vargas EA. Stability analysis of a slope under impact of a rock block using the generalized interpolation material point method (GIMP). Landslides 2019;16:751–64.
[31] Zhang D, Ma X, Giguere PT. Material point method enhanced by modified gradient of shape function. J Comput Phys 2011;230(16):6379–98.
[32] Nguyen-Thanh N, Li W, Zhou K. Static and free-vibration analyses of cracks in thin-shell structures based on an isogeometric-meshfree coupling approach. Comput Mech 2018;62(6):1287–309.
[33] Li W, Nguyen-Thanh N, Zhou K. Adaptive analysis of crack propagation in thin-shell structures via an isogeometric-meshfree moving least-squares approach. Comput Meth Appl Mech Eng 2020;358(1):112613.
[34] Nguyen-Thanh N, Huang J, Zhou K. An isogeometric-meshfree coupling approach for analysis of cracks. Int J Numer Meth Eng 2018;113(10):1630–51.
[35] Nguyen-Thanh N, Kun Z. An adaptive extended isogeometric analysis based on PHT-splines for crack propagation. Int J Numer Meth Eng 2017;112 (12):1777–800.
[36] Nguyen-Thanh N, Li W, Huang J. Adaptive higher-order phase-field modeling of anisotropic brittle fracture in 3D polycrystalline materials. Comput Meth Appl Mech Eng 2020;372(1):113434.
[37] Li W, Nguyen-Thanh N, Zhou K. Phase-field modeling of brittle fracture in a 3D polycrystalline material via an adaptive isogeometric-meshfree approach. Int J Numer Meth Eng 2020;121(22):5042–65.
[38] Yang S, Ren X, Zhang J. Study on hydraulic fracture of gravity dam using the numerical manifold method. Rock and Soil Mechanics 2018;39(8):3055–60.
[39] Zhou X, Shou Y, Qian Q. Three-dimensional nonlinear strength criterion for rock-like materials based on the micromechanical method. Int J Rock Mech Min Sci 2014;72:54–60.
[40] Zhang H, Wang K, Chen Z. Material point method for dynamic analysis of saturated porous media (II): dynamic contact analysis between saturated porous media and solid bodies. Chinese J Geotech Eng 2009;31(11):1672–9.
[41] Gingold RA, Monaghan JJ. Smoothed particle hydrodynamics: theory and application to non-spherical stars. MNRAS 1977;15(3):375–89.
[42] Lucy L. A numerical approach to the testing of the fission hypothesis. Astron J 1977;82(12):1013–24.
[43] Dalrymple RA, Rogers BD. Numerical modeling of water waves with the SPH method. Coast Eng 2006;53(2):141–7.
[44] Potapov S, Maurel B, Combescure A. Modeling accidental-type fluid–structure interaction problems with the SPH method. Comput Struct 2009;87(11):721–34.
[45] Zhao Y, Zhou X, Qian Q. Progressive failure processes of reinforced slopes based on general particle dynamic method. Journal of Central South University 2015;22(10):4049–55.
[46] Zhou X, Zhao Y, Qian Q. Numerical simulation of rock failure process in uniaxial compression using smoothed particle hydrodynamics. Chinese J Rock Mech Eng 2015;34:2647–58.
[47] Bi J, Zhou X. Numerical Simulation of Zonal Disintegration of the Surrounding Rock Masses Around a Deep Circular Tunnel Under Dynamic Unloading. Int J Comput Meth 2015;12(3):1550020.
[48] Bi J, Zhou X, Qian Q. The 3D Numerical Simulation for the Propagation Process of Multiple Pre-existing Flaws in Rock-Like Materials Subjected to Biaxial Compressive Loads. Rock Mech Rock Eng 2016;49(5):1611–27.
[49] Bi J, Zhou X. A Novel Numerical Algorithm for Simulation of Initiation, Propagation and Coalescence of Flaws Subject to Internal Fluid Pressure and Vertical Stress in the Framework of General Particle Dynamics. Rock Mech Rock Eng 2017;50(7):1–17.
[50] Libersky LD, Petschek AG. Smoothed particle hydrodynamics with strength of materials. In: Lecture Notes in Physics. Berlin Heidelberg: Springer; 1990. p. 248–57.
[51] Libersky LD, Petschek AG, Carney TC, Hipp JR, Allahdadi FA. High strain Lagrangian hydrodynamics: A three-dimensional SPH code for dynamic material response. J Comput Phys 1993;109(1):67–73.
[52] Vonneumann J, Richtmyer R. A Method for the Numerical Calculation of Hydrodynamic Shocks. J Appl Phys 1950;21(3):232–40.
[53] Monaghan JJ. Simulating free surface flows with SPH. J Comput Phys 1994;110 (2):399–406.
[54] Yang Y, Tang X, Zheng H, Liu Q, He L. Three-dimensional fracture propagation with numerical manifold method. Eng Anal Boundary Elem 2016;72:65–77.
[55] Monaghan JJ, Gingold RA. Shock simulation by the particle method SPH. J Comput Phys 1983;52(2):374–89.
[56] Zhang Z, Jin X, Luo W. Numerical study on the collapse behaviors of shallow tunnel faces under open-face excavation condition using mesh-free method. J Eng Mech 2019;145(11):04019085.
[57] Liu L, Li H, Li X. Full-field strain evolution and characteristic stress levels of rocks containing a single pre-existing flaw under uniaxial compression. Bull Eng Geol Environ 2020;79(4):3145–61.
[58] Bobet A, Einstein H. Fracture coalescence in rock-type materials under uniaxial and biaxial compression. Int J Rock Mech Min Sci 1998;35(7):863–88.
[59] Huang C, Yang W, Duan K, Fang L, Wang L, Bo C. Mechanical behaviors of the brittle rock-like specimens with multi-non-persistent joints under uniaxial compression. Constr Build Mater 2019;220(9):426–43.